PNAS RESEARCH ARTICLE | ENVIRONMENTAL SCIENCES

Mechanistic links between physiology and spectral reflectance enable previsual detection of oak wilt and drought stress

Gerard Sapes[a,b,1], Lucy Schroeder[c], Allison Scott[a], Isaiah Clark[a], Jennifer Juzwik[d], Rebecca A. Montgomery[e], J. Antonio Guzmán Q[a], and Jeannine Cavender-Bares[a,1]

Edited by James Ehleringer, The University of Utah, Salt Lake City, UT; received September 17, 2023; accepted December 11, 2023

Tree mortality due to global change—including range expansion of invasive pests and pathogens—is a paramount threat to forest ecosystems. Oak forests are among the most prevalent and valuable ecosystems both ecologically and economically in the United States. There is increasing interest in monitoring oak decline and death due to both drought and the oak wilt pathogen (*Bretziella fagacearum*). We combined anatomical and ecophysiological measurements with spectroscopy at leaf, canopy, and airborne levels to enable differentiation of oak wilt and drought, and detection prior to visible symptom appearance. We performed an outdoor potted experiment with *Quercus rubra* saplings subjected to drought stress and/or artificially inoculated with the pathogen. Models developed from spectral reflectance accurately predicted ecophysiological indicators of oak wilt and drought decline in both potted and field experiments with naturally grown saplings. Both oak wilt and drought resulted in blocked water transport through xylem conduits. However, oak wilt impaired conduits in localized regions of the xylem due to formation of tyloses instead of emboli. The localized tylose formation resulted in more variable canopy photosynthesis and water content in diseased trees than drought-stressed ones. Reflectance signatures of plant photosynthesis, water content, and cellular damage detected oak wilt and drought 12 d before visual symptoms appeared. Our results show that leaf spectral reflectance models predict ecophysiological processes relevant to detection and differentiation of disease and drought. Coupling spectral models that detect physiological change with spatial information enhances capacity to differentiate plant stress types such as oak wilt and drought.

drought | oak wilt | previsual detection | spectral reflectance | tree mortality

Significance

The oak wilt pathogen is one of the most destructive threats to oaks in North America. Millions of dollars are invested annually to manage and mitigate its spread. Drought stress is also a leading cause of tree death and ecosystem collapse in oak-dominated forests. Both disturbances simultaneously impact forests across large spatial scales making early detection and management extremely challenging. We developed remote sensing tools to detect oak wilt and drought before visual symptoms appear and differentiate these dual stresses by integrating anatomical, physiological, and spectroscopic information from cellular to canopy levels. Previsual detection of oak wilt when followed by rapid treatment response will reduce incidence, spread, and impact of oak wilt in forest landscapes.

Forests provide critical ecosystem services including habitat for organisms, regulation of climate and air quality, erosion control, and maintenance of global biogeochemical cycles (1). Multiple global change factors threaten the health of these ecosystems due to rising abiotic and biotic stress (2). In particular, ongoing climate warming is contributing to increased tree mortality through compounded heat and drought stress (3), making forests more vulnerable to biotic agents (4). Increasing human mobility across the globe has heightened vulnerability to biotic stress through greater exposure to invasive species (5). In North American forests, invasive pests and pathogens have severely impacted tree species due to increased global warming, drought, and trade. Protecting forest ecosystems from current and future abiotic and biotic threats is one of the most pressing challenges of our time (1). Developing methods for accurate and early detection of tree decline is critical to manage forests and part of an urgent global effort to integrate remote sensing and ground-based tools to monitor changes in biodiversity for planetary stewardship (6).

Oak-dominated forests are the most abundant forest type in the conterminous United States and are critical to maintain ecosystem services in North America, but they face compounding threats of increasing heat, drought, insect pests, and tree pathogens (7). Local, state, and federal governments in the United States invest hundreds of millions annually to manage and mitigate the impacts of these threats. Given the ecological and economic importance of oak forests, it is critical to understand where these forests are at risk of widespread decline due to drought and diseases—especially as the atmosphere becomes hotter and drier—to manage the spread and impacts of pathogens. Satisfying this need requires 1) mechanism-based remote sensing tools that can predict forest health across space, time, and environments; 2) early detection capabilities to locate abiotic and biotic stressors rapidly and efficiently; and 3) capacity to distinguish stress types.

Among the many invasive pathogens that threaten oak forests, oak wilt caused by *Bretziella fagacearum* is considered one of the most destructive threats to oaks in the Eastern United States (8). The disease has been documented in 24 eastern states (9) and its intensification is annually monitored in affected regions (8). The pathogen has severely affected the more

Author contributions: G.S., J.J., R.A.M., and J.C.-B. designed research; G.S., L.S., A.S., I.C., J.J., J.A.G.Q., and J.C.-B. performed research; G.S. and J.A.G.Q. analyzed data; J.C.-B., J.J., and R.A.M., obtained funding; and G.S., L.S., J.J., R.A.M., J.A.G.Q., and J.C.-B. wrote the paper.

The authors declare no competing interest.

This article is a PNAS Direct Submission.

[1]To whom correspondence may be addressed. Email: gsapes@ufl.edu or cavender@umn.edu.

This article contains supporting information online at https://www.pnas.org/lookup/suppl/doi:10.1073/pnas.2316164121/-/DCSupplemental.

Published February 5, 2024.

vulnerable red oak lineage (*Quercus* section *Lobatae*) throughout the disease range. Red oak species fail to defend against and contain the disease once they are infected (10–12). The oak wilt pathogen spreads belowground to neighboring trees through grafted roots and aboveground by insect vectors (nitidulid beetles and oak bark beetles) that disperse the spores over short to long distances (10). Long-distance dispersal poses serious challenges to track or predict the advance of oak wilt; thus, early detection of the disease across the landscape is required to limit disease spread. Accurate detection of oak wilt also requires differentiating its symptoms from those caused by other stressors such as drought, which can be confused with oak wilt (13). While spectral reflectance has been used to detect oak wilt in mature trees (14) and to differentiate oak wilt from drought in greenhouse-grown seedlings (13), previsual detection of the disease and differentiation from drought in an outdoor context has yet to be achieved. In this paper, we link physiology and remote sensing across spatial scales using proximal and drone-retrieved spectral signals to detect oak wilt and drought stress before visual symptoms appear and to differentiate both types of stress in an outdoor potted experiment. We validate the approach in a field experiment on naturally occurring saplings inoculated with the pathogen.

Remotely sensed plant spectral reflectance is increasingly used to detect abiotic and biotic stress in ecosystems at local and landscape scales. Spectral reflectance has been successfully used to detect disease and insect pest damage such as rapid ohia death, emerald ash borer, bark beetles, olive decline due to *Xylella fastidiosa*, *Phytophthora*-induced decline of Holm oak as well as oak wilt (15–23). Drought stress can also be detected spectrally at leaf to landscape scales (24–29). While studies on the detection of these stress types are increasing, only a handful of studies show early detection capacity (i.e., limited symptoms in tree crowns) (26, 30) and even fewer show previsual detection capabilities (19, 31). Underlying this gap is a lack of reflectance datasets associated with 1) the transition between non-stressed and slightly stressed plants and 2) the physiological processes underlying this transition such as photosynthetic decline, turgor loss, dehydration, cell content leakage, and cell death (4, 32–35). A focus on the onset of plant stress is therefore key to understanding which spectrally predicted physiological processes might indicate abiotic and biotic stress before visible symptoms appear. Of the physiological processes associated with plant stress and mortality, only photosynthetic declines, and dehydration have been previously linked to spectral features (29, 36). Yet, turgor loss, cell leakage, and death can likely be spectrally detected due to structural and chemical alterations in cells and tissues and used to inform stress detection at larger scales of canopy, stand, and landscape.

Studying previsual detection of any stress is challenging because the observed data necessary to construct detection models must meet two requirements. First, it is necessary to frequently monitor and document changes in visual symptoms throughout the process of stress-induced plant decline. These data enable us to represent time relative to the first appearance of visual symptoms instead of time since pathogen inoculation or since the start of an experiment. Representing timing in terms of symptom appearance is key to identify which physiological processes are impaired before visual symptoms of stress appear. Biologically based temporal variables such as time since visual symptom appearance also reduce plant-to-plant variation that is not relevant to previsual detection by accounting for individual differences in time to symptom appearance due to plant size, ontogeny, morphology, or environmental heterogeneity (37). Second, it is necessary to measure the candidate early detection predictors before, during, and after the onset of visual symptoms at high frequency and with large sample sizes. These are critical to capture and accurately model the transition from healthy to declining plant status. An approach based solely on stress-specific physiological mechanisms might allow for previsual detection of causal stressors such as drought and oak wilt. However, physiological measurements are time consuming and often destructive, thus precluding high-frequency sampling and large sample sizes. In contrast, physiological status estimated from rapid and non-destructive observations of spectral reflectance has the potential to overcome these constraints.

Oak wilt and drought-stressed oaks show similar progression of symptoms because both stressors involve impairment of vascular function. Under soil and/or atmospheric drought, water transport through the xylem is reduced causing declines in turgor pressure, stomatal conductance, and transpiration rates (38–40). Severe drought triggers embolism formation followed by tissue dehydration, cell damage, cell content leakage, and eventually plant death (4, 41–43). Infection of oaks by *B. fagacearum* also reduces water transport through the xylem but does so because of induced tylose formation rather than embolism. Tyloses are balloon-like defense structures that irreversibly occlude vessels in response to the presence of the fungus (10, 12). Tyloses can slow down the spread of the fungus within a tree, but occluded vessels lose function and prevent long-distance transport of water to the leaves, leading to reduced photosynthesis and transpiration similar to drought-stressed trees. The overlap in physiological decline processes between oak wilt and drought makes it challenging to distinguish these two stressors. However, we expect that differences in the cause of xylem dysfunction (i.e., emboli vs. tyloses) and how they are generated (i.e., xylem tension vs. fungal infection) provide the mechanistic information necessary to distinguish between oak wilt and drought.

The spatial patterning of xylem dysfunction likely differs between oak wilt and drought-obstructed vessels. Vascular wilts like oak wilt obstruct vessels following infection (44, 45) such that vessels become obstructed by tyloses as they come into contact with the fungus. As such, xylem dysfunction develops from the point of pathogen entry inwards, forming clusters of occluded vessels. Drought stress obstructs vessels by formation of emboli, which form as a function of vessel vulnerability to tension and tend to occur first in larger vessels (46). Vessel sizes in ring-porous oaks vary radially from large to small within a given annual growth ring across the entire cross-section of a stem, such that xylem dysfunction due to drought tends to progress radially rather than developing locally around a pathogen-colonized area, as in the case of oak wilt. Spatial patterns of physiological decline in tree canopies likely mirror spatial patterns of xylem dysfunction because they result from loss of water transport in the vessels that supply the leaves. Consequently, oak wilt–infected trees might show clustered physiological decline in the canopy with some branches affected while others remain healthy. This would result in high within-canopy variability in symptoms. In contrast, drought-stressed trees might show more widespread physiological decline across the canopy (i.e., low within-canopy variability). Because physiological decline can be correlated with and detected using spectral reflectance data, we test whether spatially explicit spectral data obtained using low-cost multispectral cameras mounted on unoccupied aerial vehicles (UAVs) can detect spatial patterns of stress that differentiate oak wilt and drought. However, the links between both physiological mechanisms and processes and spectral reflectance across spatial scales necessary to evaluate the potential of multispectral UAVs as tools to detect drought and oak wilt have yet to be resolved.

Here, we aimed to 1) determine which physiological processes are impacted as the plant loses function and which can be estimated through plant spectral reflectance (Fig. 1, O1), 2) identify which of these spectrally predicted physiological processes can detect oak wilt and drought before visual symptoms appear (Fig. 1, O2), and 3)

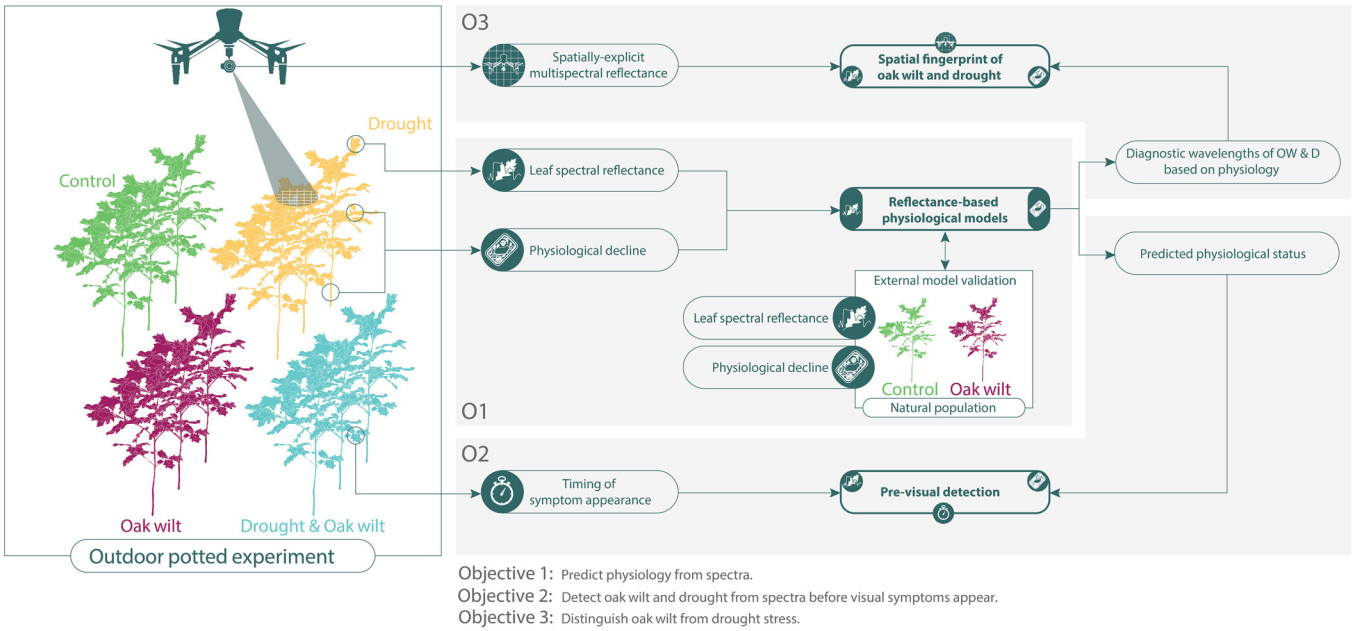

Fig. 1. Logic schematic of the experimental design, questions, and methodological approach. The panel on the left depicts treatment groups and methods of spectral imaging, both at the canopy and the leaf level. Each of the gray boxes indicates the approach taken to answer the three main objectives which are (O1) Predict physiology from spectra, (O2) detect oak wilt and drought from spectra before visual symptoms appear, and (O3) distinguish oak wilt from drought stress.

find spectral indices that are compatible with low-cost multi-spectral UAV sensors that capitalize on physiologically informative wavelengths to detect and differentiate oak wilt from drought (Fig. 1, O3). We hypothesized that i) processes of plant dysfunction such as dehydration, cellular death, and cell content leakage can be spectrally detected due to their impacts on tissue structure and chemistry, ii) physiological measurements related to cell death would detect oak wilt and drought before visible symptoms appear, and iii) trees infected with the oak wilt pathogen would show higher within-canopy physiological variability than droughted trees when observed through UAV spectral indices related to cell damage and death.

Results

Physiological Progression of Oak Wilt and Drought Stress. In all treatments of the potted sapling experiment, physiological state remained similar to the control group (C, Fig. 2 violin plots) values until visual symptoms appeared (Fig. 2, day 0 vertical line). Right before visible symptoms appeared, we observed slight increases in electrolyte leakage (EL, Fig. 2*A*) and in loss of rehydration capacity (LRC, Fig. 2*F*), as well as slight declines in relative and volumetric water content (RWC and VWC, Fig. 2 *D* and *E*) in all treatments. In the case of midday water potential (Fig. 2*G*), only drought (D) and drought combined with oak wilt (DxOW) showed slight declines before visible symptoms appeared. Maximum efficiency of photosystem II (Fv/Fm, Fig. 2*C*) showed the earliest decline of all physiological variables measured. However, for all variables, CI were too wide to ascertain previsual detection capacity. After visible symptoms appeared, D, OW, and DxOW treatments showed sharp increases in EL and LRC and sharp declines in RWC, VWC, and water potential (*P*-value range: 0.022 to <0.001). Importantly, there were no significant differences in physiological progression between D, OW, and DxOW treatments.

Spectral Reflectance Progression of Oak wilt and Drought Stress. In the potted sapling experiment, we observed increasingly significant shifts across several wavelength regions of the canopy spectra as oak wilt and drought stress visual symptoms increased in severity (Fig. 3 *A* and *B* and *SI Appendix*, Appendix S6). The first shifts in spectral reflectance appeared in canopies 33 d after imposing treatments. In OW trees, canopy spectral reflectance first increased at 1,400 to 1,500 nm within the short-wave infrared (SWIR) ($P < 0.01$). The red edge region declined at 700 to 750 nm at 48 d ($P < 0.01$). By day 62, nearly the full spectral range was different than controls except for the green region of the visible range (VIS), some areas of the red edge, and SWIR wavelengths around 1,600 nm. In D trees, canopy spectral reflectance first decreased at ca. 1,150 nm of the NIR ($P < 0.01$) and those detected in OW by day 33. After 48 d, significant wavelengths were found in the blue and red VIS regions, between 1,000 to 1,270 nm, 1,400 to 1,500 nm, and 1,950 to 2,200 nm ($P < 0.01$). After 62 d, nearly the full spectral range was different like in the case of OW ($P < 0.01$). DxOW also manifested changes at 33 d; significant wavelengths were a combination of the first wavelengths detected in OW and D trees, plus a region at 1,600 to 1,750 nm ($P < 0.01$). By day 48, DxOW trees showed significant wavelengths across the whole spectral range ($P < 0.01$) similar in direction and magnitude to those observed in OW trees by day 62.

Shifts in leaf spectral reflectance lagged those of canopy reflectance. Although the shape of the spectra was already changing by 33 d, we did not observe significant differences until 62 d because we set our alpha threshold at 0.01. At 62 d, we observed increases in the VIS range, declines in reflectance across and beyond the VNIR range (750 to 1,300 nm), and increases at the SWIR range ($P < 0.01$) of the spectra (Fig. 3-IV-A). D leaves first showed increased reflectance at the red region of the VIS ($P < 0.01$) by day 33. The blue and the 750 nm regions increased and decreased ($P < 0.01$) respectively, and reflectance at the SWIR water bands increased ($P < 0.01$) by day 48. Nearly the full range of the spectra of D leaves was different than controls by day 62. DxOW leaves went from no difference from controls to suddenly being the most spectrally different, with nearly all regions of the spectra showing significant differences by day 62 ($P < 0.01$).

Predicting Physiology from Spectra. PLSR models based on leaf spectral reflectance predicted relative and volumetric water content (RMSEP = 11.47%, 10.76% respectively), loss of rehydration

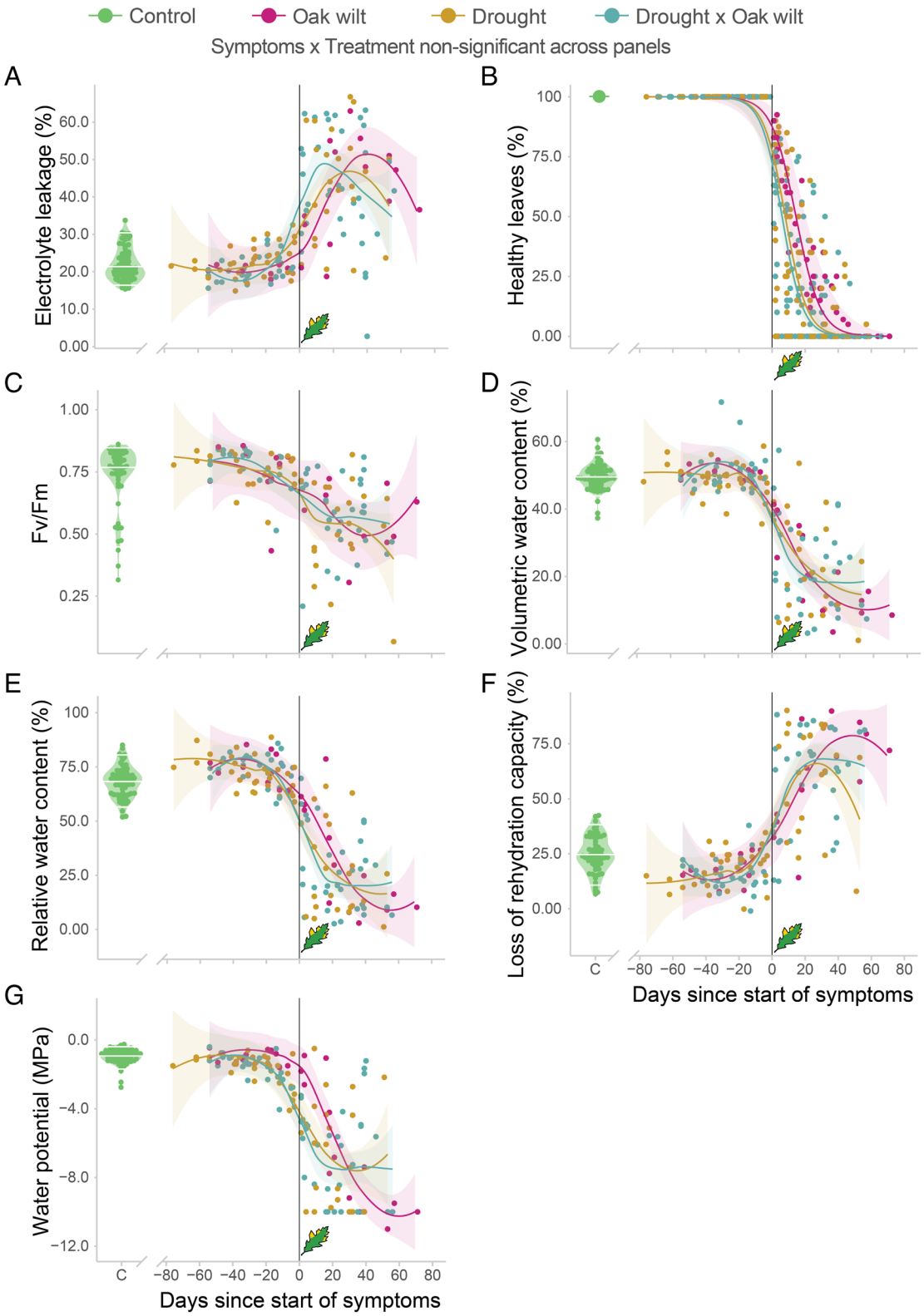

Fig. 2. Progression of physiological symptoms in oak wilt (OW), drought (D), and drought plus oak wilt (DxOW) treatments. The violin plots in green indicate the median and range of physiological status observed in the control group (C in the x axis) across the duration of the experiment. The black vertical line and leaf icon at day 0 indicate the start of visual symptoms. Electrolyte leakage (*A*) increases before visual symptoms appear in the form of non-healthy leaves (i.e., wilted, brown edges, or dry), as indicated in the decline in healthy leaves (*B*). Fv/Fm (*C*), volumetric water content (*D*), and relative water content (*E*) decline before symptom appearance. Loss of rehydration capacity (*F*) increases, and water potential (*G*) declines before the start of symptoms. All panels show statistically significant effects of days since start of symptoms on the response variables, but we did not detect significant differences in slopes among treatments.

capacity and electrolyte leakage (RMSEP = 11.98%, 13.09% respectively), water potential (RMSEP = 19.77%), and maximum efficiency of photosystem II (RMSEP = 16.16%) both when all trees were used and when controls were excluded (*SI Appendix*, Appendix S7). When applied to data from the outdoor potted experiment not used to train models (cross-validation), measured

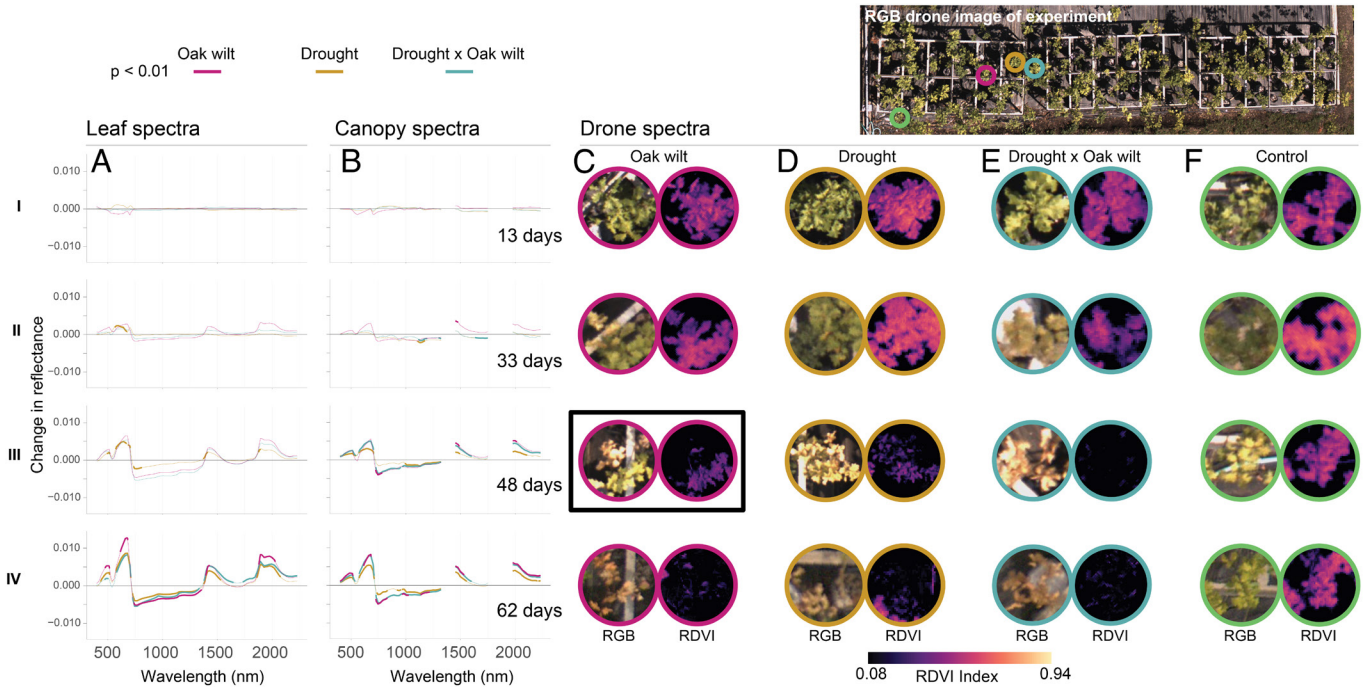

Fig. 3. Repeated measurements of leaf- (*A*), canopy- (*B*), and UAV-measured spectra (*C*–*F*) over the course of stress progression allowed identification of wavelengths indicative of oak wilt (OW) and drought (D) stress at different stages of physiological decline. The heterogenous physiological decline within canopies of oak wilt trees during early stages of infection can be clearly observed in the UAV-measured re-normalized difference vegetation index (RDVI) images at 48 d since the start of the experiment (black box in C III), but decline was already noticeable at 33 d (black box in C III). Note that 33 d corresponds to the date in which visible symptoms of stress appeared for the oak wilt–infected tree shown in the outlined box. Columns (*A* and *B*) show the difference in normalized reflectance between control and treated trees at each date (13, 33, 48, and 62 d) since the start of the experiment. Bolded line segments in columns (*A* and *B*) show wavelengths with significant ($P < 0.01$) changes over time.

vs predicted plots showed similar slopes among treatments (Fig. 4 *A*, *C*, *E*, and *G*) which indicated that physiological status was predicted with similar bias regardless of the type of stress. When models were independently validated with measurements from a natural population of red oaks inoculated with *B. fagacearum* at Cedar Creek, spectrally predicted VWC and Fv/Fm nicely tracked the measured values both in control and oak wilt diseased trees (Fig. 4 *B* and *D*). VWC and Fv/Fm of the diseased trees diverged from controls (no overlap in CI) before visible symptoms appeared (day 22 after inoculation) in both measured and spectra-predicted values. Spectra-predicted VWC and Fv/Fm also tracked a slight recovery in VWC and Fv/Fm that occurred after a rain pulse around day 70 after inoculation. Based on the success of VWC and Fv/Fm spectral models to predict measured values at Cedar Creek, we decided to apply two other spectral models (LRC and EL) that showed good cross-validation performance to the Cedar Creek dataset. While we did not measure LRC and EL at Cedar Creek to validate predictions, spectrally predicted LRC and EL in these plants showed clearly distinct patterns between oak wilt diseased and control trees (Fig. 4 *F* and *H*).

Distinguishing Oak Wilt from Drought Stress in Xylem and Canopies. Trees infected with *B. fagacearum* that showed no visual symptoms by the end of the experiment (asymptomatic) retained some of their xylem functional, but less than controls ($P < 0.05$), whereas symptomatic trees lost all their functional xylem ($P < 0.001$, and *SI Appendix*, Appendix S9). Xylem occluded by tyloses could not be removed by flushing, whereas embolisms caused by drought could be flushed ($P < 0.05$, Fig. 5*C*), differentiating hydraulic dysfunction caused by drought from that caused by oak wilt. Hydraulic dysfunction associated with oak wilt showed a spatial pattern typical of a pathogen that is carried in the transpiration stream from a point of infection (or artificial inoculation) toward contiguous sections of the xylem; whereas drought-affected trees showed no spatial pattern ($P < 0.001$, Fig. 5*C*). Trees subjected to both drought and oak wilt (DxOW) exhibited xylem occlusion levels intermediate to those of D and OW trees and were not significantly different from either group ($P > 0.05$, Fig. 5*C* and *SI Appendix*, Appendix S9). These DxOW trees exhibited both contiguous and non-contiguous hydraulic dysfunction, covering the range of responses observed in both D and OW trees. However, their spatial pattern was statistically most similar to that of D trees.

The average canopy pixel value from the UAV sensor for the re-normalized difference vegetation index (RDVI), which uses key wavelengths identified by our spectrally predicted physiological models (*SI Appendix*, Appendix S7), declined in OW, D, and DxOW trees as drought and oak wilt progressed (Fig. 3 *C*–*F*, I-IV). However, the within-canopy SD in RDVI increased in OW trees relative to D trees as the disease progressed and visible symptoms appeared ($P = 0.02$, Fig. 5*B*).

Detecting Oak Wilt and Drought Stress Before Visible Symptoms Appear. Bayesian segmented regressions identified an inflection point corresponding to the day at which spectrally predicted physiology started to change in response to stress (Fig. 6*A*). Fv/Fm had the highest previsual detection capacity, showing spectrally predicted Fv/Fm declines in D, OW, and DxOW treatments at about 11, 12, and 6 d (respectively), but up to 27, 24, and 12 d (respectively) before visible symptoms appeared (Fig. 6*B* and *SI Appendix*, Appendix S10). LRC could also detect drought and oak wilt before visible symptoms appeared. On average, increases in LRC could be spectrally detected in D, OW, and DxOW treatments about 8, 6, and 5 d, but up to 15, 11, and 9 d (respectively), before visible symptoms appeared. Water potential, VWC, RWC, and EL could previsually detect D and DxOW stress within similar timeframes as LRC. However, in trees of the OW

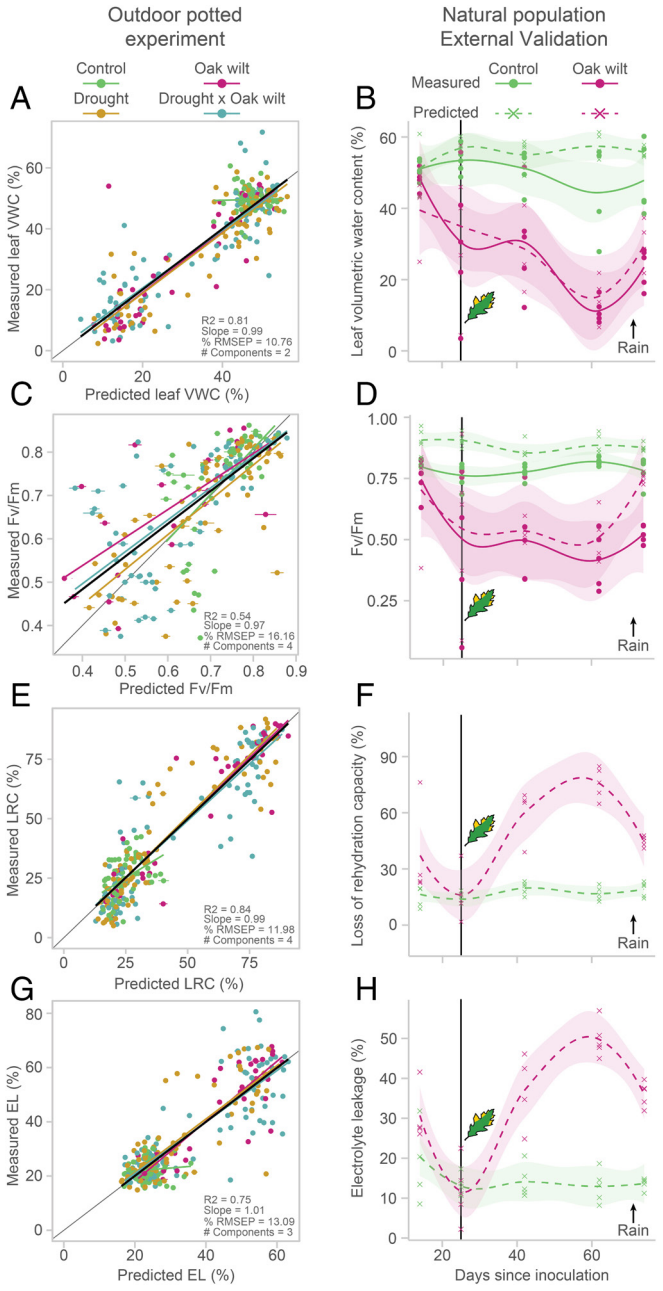

Fig. 4. Predictions of physiology from spectral reflectance using PLSR models. Measured vs. predicted plots (left) and validation plots (right) for volumetric water content (*A*, *B*), Fv/Fm (*C*, *D*), loss of recovery capacity (*E*, *F*), and electrolyte leakage (*G*, *H*). On the measured vs. predicted plots, the thin, gray line indicates a 1:1 fit. The black line indicates the overall model fit across treatments. All other lines represent the overall model fit within each treatment and are colored according to their treatment (control=green, oak wilt=purple, drought=gold, drought X oak wilt=blue). On the validation plots, the models were validated using an external dataset from the Cedar Creek natural population field experiment. Circles indicate the measured values, and crosses indicate the predicted values. A leaf icon and black vertical line indicate the date of visual symptoms detected. An arrow indicates the date of a rain event that led to a recovery of function.

treatment, their detection threshold was not significantly different from the day of visible symptom appearance.

Discussion

A long-standing challenge in remote sensing of plant stress is to detect and differentiate stress types by causal factor early enough to improve efficacy of local site treatments for disease management. Our results show that leaf spectral reflectance can detect oak wilt and drought more than 1 wk before visual symptoms appear and can differentiate the two stressors. Accurately differentiating oak wilt symptoms from drought-induced stress requires coupling leaf spectra to the physiological processes and mechanisms underpinning each causal factor to identify wavelengths associated with early physiological decline. We find that spatial patterns of spectral indices sensitive to oak wilt and drought can help differentiate these stresses using relatively low-cost multi-spectral UAV sensors. Our results highlight the importance of mechanistically linking characteristics derived from remote sensing to physiological processes to improve monitoring of forest health.

Reflectance-Based Physiological Models Detect Oak Wilt and Drought. Physiological processes linked to photosynthesis, dehydration, and cell death can be predicted from leaf spectral reflectance. Declining turgor and stomatal closure are the first processes to occur in oak wilt and drought-stressed oak seedlings (13). In trees infected with *B. fagacearum*, these changes result from clogged conduits (Fig. 5*C*) (10). In drought-stressed trees, decreased turgor and closure of stomata occur due to decreasing water potentials triggered by water deficit (4). Prolonged stomatal closure eventually impacts chlorophyll concentrations, manifested in leaf spectra as an increase in reflectance at red and blue wavelengths (47). Increases in reflectance at red and blue wavelengths are among the first to occur in oak wilt and drought-stressed trees (Fig. 3*A* and *SI Appendix*, Appendix S6) and are a strong predictor of physiological processes linked to photosynthesis such as maximum quantum efficiency of Photosystem II (Fv/Fm) (*SI Appendix*, Appendix S8). After photosynthetic inhibition and turgor loss, leaves continue to dehydrate and start to experience permanent and irreparable damage to cell walls due to cellular collapse (i.e., cytorrhysis, which causes loss of rehydration capacity) (42). Cellular contents leak through degraded membranes, and cells die (*SI Appendix*, Appendix S8). Dehydration, cytorrhysis, and cell leakage all increased leaf reflectance across wavelengths that are absorbed by water and decreased reflectance across wavelengths sensitive to changes in cell mesophyll structure and pigment content (*SI Appendix*, Appendies S6 and S8). Cytorrhysis and cell leakage are processes that occur nearly simultaneously due to dehydration (42). As such, they occur at similar times relative to the onset of visible symptoms for both oak wilt and drought (Fig. 2).

The reflectance-based models that we built to predict these physiological processes were trained in a controlled experimental setup with one species (*Quercus rubra*). Yet, they detected physiological stress caused by oak wilt in the field despite the variability inherent to natural communities with mixed species—two red oak species (*Q. rubra* and *Q. ellipsoidalis*) in our case—and uneven ages (Fig. 4). Predicted vs measured values showed variability at intermediate values of the measured physiological range. This could occur because spectral reflectance is not a perfect predictor of physiological characteristics or due to within-leaf variability in physiology and spectra. Within-leaf variability is captured by the small field of view of the fiber optic but not by physiological measurements that are measured at the whole leaf level. Covering a wide range of physiological values during model training ensured that measured vs predicted slopes remained close to the 1:1 line and intermediate values could be accurately predicted. Accordingly, spectrally predicted physiology at the Cedar Creek experiment tracked measured physiology even at intermediate values of the measured range of the testing data (Fig. 4 *B* and *D*). We were also able to distinguish trees infected with *B. fagacearum* from healthy trees based on LRC and EL models despite having no physiological

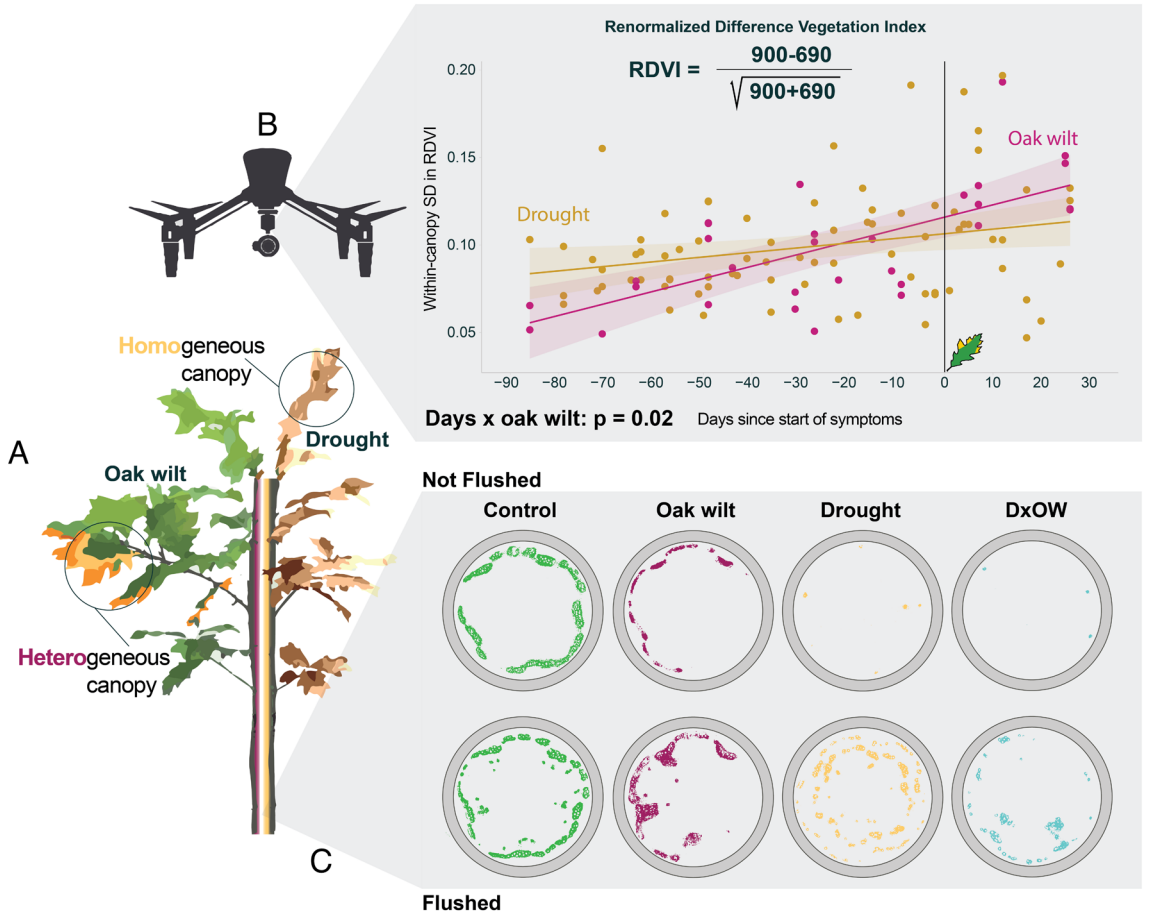

Fig. 5. Oak wilt–infected canopies are more physiologically heterogeneous than drought-stressed canopies (panel *A*). This heterogeneity can be spatially detected by measuring within-canopy variability using UAVs and spectral indexes associated with physiological decline, such as the re-normalized difference vegetation index (RDVI, panel *B*). The heterogeneity is caused by the spread of the oak wilt pathogen through the stem vascular system, blocking conduits and causing dysfunction in localized areas of the wood, as indicated by a lack of dye in areas of the stem cross sections while other areas remain functional (shown as red colored areas, panel *C*, not flushed). At early stages of infection, the localized dysfunction in the xylem leads to localized physiological decline in the canopies. This is because some branches and the leaves they support are connected to blocked vessels while most remain connected to functional ones. In contrast, drought reduces water flow through the vascular system as a function of conduit size because wide vessels are often more vulnerable to bubble formation and cavitation. Drought thus generates a non-localized pattern of loss in xylem function (yellow coloring shows the small number of functional xylem vessels under drought stress, and blue coloring shows the still smaller number of functional vessels under drought and oak wilt stress, panel *C*, not flushed). Drought-induced air bubbles can be flushed out with high-pressure dye-infused water while blockages from oak wilt cannot be flushed (panel *C*, flushed).

observations for these variables in the field (Fig. 4 *F* and *H*). These results suggest that reflectance-based physiological models provide lower risk of faulty extrapolation and higher chance of success than models that do not have a physiological basis when applied to new locations, periods, or species. Our findings indicate that spectroscopic models of plant stress that are grounded in the physiological mechanisms and processes that plants undergo during oak wilt disease progression and drought can produce general insights.

Oak Wilt and Drought Can Be Detected More Than a Week before Visual Symptoms Appear. While all spectrally predicted physiological processes were able to detect drought stress before visual symptoms appeared, only Fv/Fm and loss of rehydration capacity (LRC) could do so for oak wilt (Fig. 6). Fv/Fm and LRC can detect oak wilt and drought more than 1 wk before leaves exhibit visual symptoms. This is likely because they are associated with early signs of stress, such as photosynthetic declines and turgor loss (48, 49). While only two spectrally predicted physiological processes could detect oak wilt before visual symptoms appeared, all of them could detect oak wilt disease within 3 d after the first leaf showed visual symptoms in a tree (Fig. 6). Landscape detection of oak wilt by ground detection surveys (GDS) conducted by personnel trained to recognize visual crown symptoms and other site clues are labor intensive, slow, and based on advanced crown symptoms (e.g., >30% of crown affected) (10). Close examination of suspect trees by GDS is required to differentiate diseased and droughted trees. Aerial detection surveys monitor landscapes more quickly, but ground-truthing of suspect sites is also required if both droughted and diseased trees are present because they cannot be distinguished from the air. Management strategies can fail to contain oak wilt because the disease often has already spread via insect vectors to nearby trees by the time the symptomatic trees are correctly diagnosed and sites treated (10). Our results suggest that oak wilt and drought could be detected much earlier using spectral reflectance data from remote sensing platforms. Survey crews could monitor larger areas with fewer people and quickly respond with treatments before the pathogen has a chance to spread. Previsual detection via spectra could also improve methods aimed at stopping pathogen spread through inter-tree root grafts. For instance, previsual detection could improve delineation of outer perimeter lines of oak wilt centers and surrounding buffers which are currently based on experience or statistical models (50) and that sometimes miss asymptomatic but already infected trees.

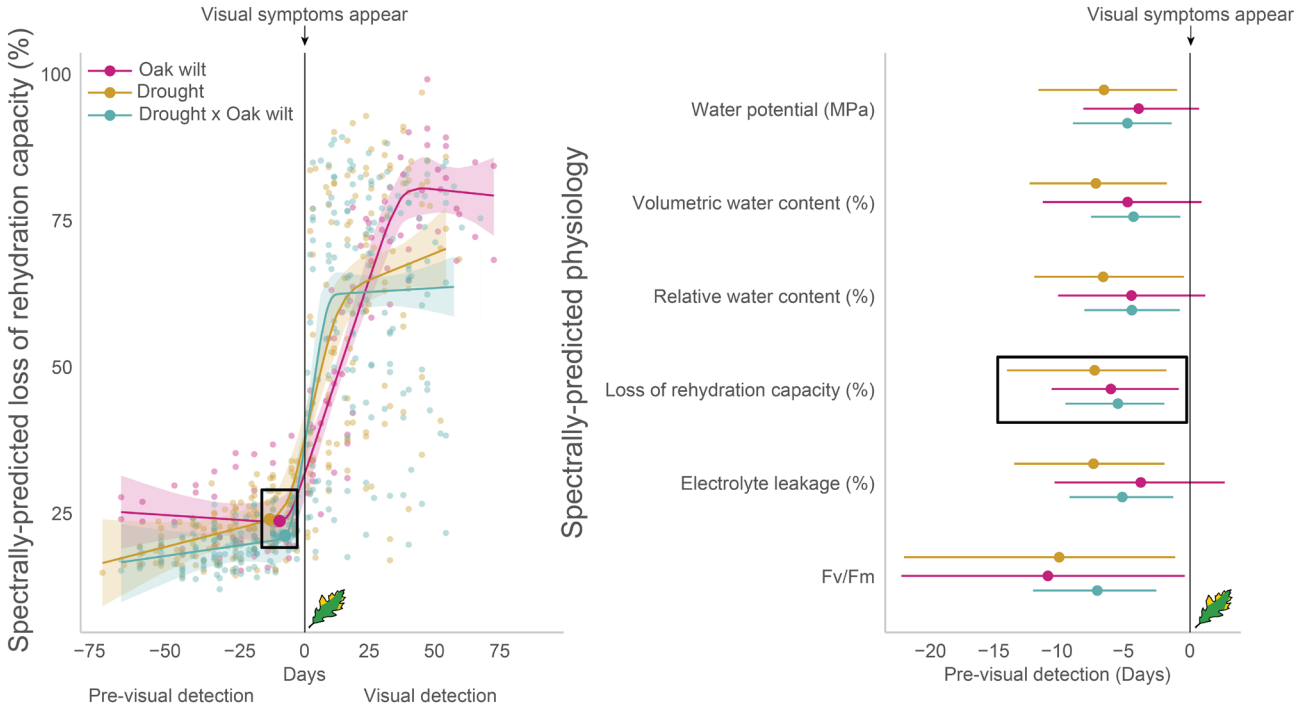

Fig. 6. *Left* panel: Bayesian segmented regressions (*Left* panel) identified inflection points (black box) corresponding to the day in which spectrally predicted physiological decline (e.g., loss of rehydration capacity associated with cell damage) started. Day 0 of the *x* axis represents the day in which visual symptoms appeared. Negative and positive values correspond to days prior and after the day of symptom appearance, respectively. If the inflection point occurs before day 0, the spectrally predicted physiological process can detect stress before visual symptoms appear. *Right* panel: Inflection points for each spectrally predicted physiological process and stress type. Lines represent CI around the predicted onset of physiological symptoms. All spectrally predicted physiological processes detected drought stress or combined drought and oak wilt stress prior to the appearance of visual symptoms (i.e., CI do not overlap with day 0, vertical black line). However, only spectrally predicted loss of rehydration capacity and Fv/Fm (related to photosynthetic activity) detected stress associated with oak wilt before visual symptoms appeared. Loss of rehydration capacity detected oak wilt between 11 to 2 d before visual symptoms appeared (average of 7), while Fv/Fm detected oak wilt between 26 to 1 d before visual symptoms appeared. Physiological changes associated with oak wilt did not always occur before visual symptoms appeared (CI overlap with the 0 d) but were still detectable as early as 3 d after visual symptoms appeared.

Currently, UAVs equipped with RGB sensors are used to detect single trees exhibiting oak wilt symptoms in forest compartments in Menominee County, WI, USA, managed by Menominee Tribal Enterprises foresters. A rapid response treatment has been devised to prevent spread of the pathogen downward into the root systems and then to adjacent trees. The treatment involves making two stem girdling cuts 15 to 25 cm apart into the outer xylem of the lower main stem of a tree exhibiting incipient wilt and applying liquid herbicide to the fresh cuts. Low-cost multispectral UAVs like ours would maximize the time window during which these treatments are effective. In terms of drought, early detection can greatly improve our ability to forecast and manage forest health under future drier conditions and, for instance, take action to increase forest defenses against biotic agents or reduce fire risk resulting from higher flammability of droughted stems.

Distinguishing Oak Wilt from Drought Requires Combining Physiology and Spectral Reflectance. The leaf-level physiological processes that trees experience as they develop oak wilt and drought symptoms (Fig. 2) are similar because the causal agent is the same: a loss of hydraulic conductivity in the xylem (Fig. 5*C*). As such, leaf-level physiology alone cannot distinguish oak wilt from drought stress. However, how loss of hydraulic conductivity manifests spatially through the xylem differs between oak wilt and drought-stressed trees (Fig. 5*C*). Loss of hydraulic conductivity in trees infected with oak wilt results in a clustered spatial pattern of xylem dysfunction that does not occur in drought-stressed trees. It is therefore possible to distinguish between oak wilt and drought using xylem staining techniques, but this approach is impractical for large-scale assessments. Yet, the spatial differences in xylem dysfunction provide the causal physiological mechanism that allows differentiation of both stressors at larger scales. Because branches in the canopy are connected to different sets of conduits at the base of the stem, trees at early stages of oak wilt crown symptom development show photosynthetic decline, dehydration, and cell death only in the subset of branches connected to occluded xylem vessels (Fig. 3*C*). This pattern generates large variability in physiological status across the canopy as symptoms develop (Fig. 5*B*). By coupling the physiological processes to spectral reflectance data, we identified wavelengths sensitive to these processes and used them to select spectral indices observable with low-cost UAVs such as the RDVI index, shown to be among the most sensitive to oak wilt (14). The wavelengths 900 and 690 nm used in this index are linked to photosynthetic activity and leaf structural integrity (51)—confirmed by our PLSR models (*SI Appendix*, Appendix S8)—which explains the sensitivity of this index. This trans-disciplinary approach enabled us to detect spatial variability in physiological status and to distinguish trees at early stages of oak wilt development from drought-stressed trees (Figs. 3 *C* and *D* and 5*B*). Our results show that it is critical to consider spatial patterns as part of a mechanistic approach at all scales (i.e., tissue, organ, and individual). Considering xylem, leaf, and canopy patterns together was essential for distinguishing oak wilt from drought. Spatial patterns are also important for detecting oak wilt at both tree and stand levels because it reduces misclassification and allows detection of oak wilt pockets (14). Because oak wilt manifests similarly across the extant range of red oaks (*Quercus* section Lobatae) (52), we are hopeful that both the patterns observed in this study and our approach will be broadly applicable.

Conclusions

Throughout the decades-long history of remote sensing, scientists have aspired to monitor plant stress from the skies with the click of a button (53)—but that day has been slow to arrive. One reason may be that remote sensing approaches frequently lack the mechanistic basis to be generalized across space, time, and biological systems (54). The field of plant ecophysiology has long claimed to provide a solid mechanistic foundation that could be used to monitor the severity of plant stress in a general way (55). However, collecting large-scale ecophysiological data at temporal and spatial resolution needed to monitor plant stress across landscapes is impractical. Our study shows that combining both disciplines, into what could be called spectral ecophysiology, provides the best of both worlds. In our case, it enabled early detection and differentiation of the biotic and abiotic stressors that cause oak wilt and drought. Ecophysiology informs which plant processes should be predicted from remotely sensed spectral reflectance. Remote sensing enables high-throughput, spatially explicit estimates of such processes. Spectrally predicted ecophysiology and spectral indices grounded in ecophysiology are tied to fundamental biology. They are therefore likely to generalize better than reflectance signals that are not connected to biological processes. We hope that our research motivates future studies to explore the linkages between ecophysiology and spectral reflectance; to discern what can—and cannot—be measured, when, and in which plant systems.

Methods

Experimental Design. In the spring of 2019 and 2021, we conducted two experiments: 1) a field experiment with naturally regenerated red oak saplings artificially inoculated with *B. fagacearum* at the Cedar Creek Ecosystem Science Reserve (45.396 N, 93.183 W, *SI Appendix*, Appendix S1) and 2) an outdoor potted experiment with *Quercus rubra* in which we applied a drought treatment and an oak wilt treatment (artificially inoculated with the pathogen) in a full-factorial design outside the Plant Growth Facilities of the University of Minnesota St. Paul Campus (44.988 N, 93.177 W).

For the Cedar Creek experiment, we selected forty naturally growing *Q. ellipsoidalis and Q. rubra* saplings with fully developed leaves. We chose a mixture of species because they are difficult to differentiate as juveniles and freely introgress. Both species are equally susceptible to oak wilt. Trees ranged from 63 to 240 cm tall with an average height of 134 cm, and basal diameters at groundline ranged from 1.2 to 5.4 cm with an average diameter of 2.8 cm. On June 27th 2019, we inoculated half of the trees (OW treatment) with *B. fagacearum* introduced as 1 mL of a homogenized aqueous spore suspension (2.1×10^5 spores $\times$ mL^{-1}) pipetted into a single freshly drilled hole (1-mm diameter $\times$ 4 cm in radial depth) placed 4 cm above the root collar. Sterile moist cotton was then placed over the wound and affixed to the stem with parafilm. The rest of the trees remained untreated as a control treatment. We tracked physiological and spectral changes in OW and C trees at 14, 25, 42, 62, and 74 d after inoculation. At each sampling date, we randomly selected five OW trees along with their nearest five control trees. This sampling scheme minimized spatial variation unrelated to the treatments.

In the outdoor potted experiment at the Plant Growth Facilities, we planted 100 bare-root saplings in pots. Trees ranged from 27 to 133 cm tall with an average height of 96 cm, and basal diameters calculated from stem perimeter at groundline ranged from 0.64 to 1.81 cm with an average diameter of 1.00 cm. On April 13 to 14, 2021, we replanted the dormant trees in 9.63L cone-shaped pots white-painted to prevent overheating of the root system and with a 2:1 mix of potting soil and sand. Trees were placed outside where they subsequently flushed prior to application of treatments. On July 15th, we inoculated half of the trees with the same inoculum concentration used at Cedar Creek. A small bark flap was cut, ring of putty applied below the cut, an aqueous suspension of inoculum introduced, and the wound covered as previously described. Half of the *B. fagacearum* inoculated trees (OW) and half of the non-inoculated trees were covered with white cling film around the base to exclude rain and induce drought. Thus, we had four treatments in a full factorial design: control (C), drought (D), oak wilt (OW), and drought and oak wilt (DxOW). Treatments were randomly distributed, and trees were evenly spaced (ca. 0.5 m apart). We tracked physiological changes in five different, randomly selected OW, D, DxOW, and C trees after inoculation on a weekly basis. Additionally, full-range spectral reflectance (400 to 2,400 nm) at both leaf and canopy levels was measured in every tree on each of the sampling days. Finally, we tracked canopy visual appearance every 3 d to identify the date on which each tree first showed visible symptoms of stress.

Sampling Procedure. In both experiments, we assessed the canopy of each tree to record the proportion of leaves at each of four symptomatic stages to identify leaves at different symptomatic stages (green, drooping, and discolored; drooping and brown edges; and entirely brown and dry). We selected representative leaves of each stage present in the target trees for physiological and spectral measurements (see below). This sampling approach was designed to ensure strong representation of the entire range of observed variation in spectra and physiology, which helps train robust spectral models. For each leaf type present, we chose a sun leaf and dark-acclimated it overnight using a light-blocking clip (Hansatech, PP Systems). The following day, we took the fluorescence in the morning and spectral measurements around midday in the selected leaves. We collected leaves and placed them in Ziploc bags containing a moist paper towel partially covered in aluminum foil to prevent desiccation without introducing external moisture into the leaf by contact with the towel (56). Leaves were then placed in a cooler and transported to the lab to measure their water status.

Chlorophyll Fluorescence, Leaf and Canopy Hyperspectral, and UAV Multispectral Reflectance. In the morning (9:00) of each sampling date and for both experiments, we measured Fv/Fm using a Hansatech chlorophyll fluorometer (PP Systems, Narborough, UK) under dark-acclimated conditions. Fv/Fm is a measure of maximum photosynthetic quantum efficiency under dark acclimated conditions and can be used to indicate leaf tissue vitality and stress (32, 57). Around midday (11:00 to 13:00), we measured full-range leaf spectral reflectance (400 to 2,400 nm) using a PSR+ 3500 instrument (Spectral Evolution, Haverhill, MA, USA) and a leaf clip, which covered a leaf surface area of ca. 1 cm^2. We also measured canopy spectral reflectance 1 m above the canopy by replacing the fiber optic probe with a 4° field of view lens. Before measuring each individual, we referenced light conditions using a Spectralon Diffuse Reflectance Standard placed directly under the fiber optic. We used R version 3.5 (58) and the *spectrolab* package (59) to import, resample every 1 nm from 400 to 2,400 nm, and normalize to a unit vector all raw spectra. Additionally, and for the outdoor potted experiment only, we flew an Unoccupied Aerial Vehicle (UAV) (DJI Inspire2) on days 13, 33, 48, and 62 of the experiment with a custom Sentera 6X multispectral camera developed in collaboration with Sentera (Saint Paul, MN). The camera measures reflectance at wavelengths 690 (±20) nm full width at half maximum, 720 (±10) nm, 760 (±10) nm, 900 (±20) nm, 970 (±40) nm, and an RGB channel. These wavelengths were selected as important in ref. 14 given VNIR sensor constraints (400 to 990 nm). Digital numbers from the multispectral images were transformed to reflectance values by the empirical line method using reflectance values from known surfaces. We used QGIS (60) and the RGB images of the UAV to manually trace canopies of each tree avoiding empty spaces in each flight date and convert them to polygons. Polygons were used to extract reflectance at each wavelength from each pixel within a canopy. Last, we calculated the re-normalized difference vegetation index (RDVI) (51) as (R900–R690)/sqrt(R900+R690), which Sapes et al. (14) showed to be highly sensitive to oak wilt. For each flight, we estimated mean and SD RDVI within each tree canopy.

Water Relations. We harvested leaves and measured midday leaf water potential (i.e., xylem tension due to water deficit) in the lab using a pressure chamber (PMS Instrument Company, Corvallis, OR, USA) following methods in ref. 61. We used the same leaves to measure volumetric (VWC) and relative water content (RWC), and percent loss of rehydration capacity (LRC). For each sampled tree, an additional leaf of each type was collected to measure electrolyte leakage (EL). Declines in both VWC and RWC and increases in EL have been associated with mortality-inducing stress (34, 35, 43); LRC has been associated with irreversible turgor loss and leaf damage (49), which also contribute to plant stress and mortality. For the sake of space, we describe methods for these measurements in *SI Appendix*, Appendix S1.

Xylem Staining. At the end of the potted experiment, we destructively sampled stem segments 30 cm above the inoculation point to assess functional and dysfunctional xylem area in a subset of trees of each treatment (9 C, 14 D, 14 OW, 22 DxOW) using the active xylem staining method (62) explained in *SI Appendix*, Appendix S1. The staining was done before and after flushing stems at high pressure to distinguish the area of xylem that was embolized from the area filled with tyloses. Conduits filled with tyloses due to oak wilt remained unstained after flushing. Because a subset of the OW trees were able to slow down the rate of within-tree colonization, we could split OW trees into symptomatic and asymptomatic. We used ImageJ (63) to measure the percent functional xylem area before flushing and the percent clogged xylem area after flushing. Additionally, we divided each cross-section into 16 sections and counted the number of contiguous obstructed xylem sections to quantify the degree of localized versus multiple xylem obstruction patterning.

Statistical Analyses.

Scaling from leaves to whole plant canopies. Both measured and spectrally predicted physiological values were scaled up to the whole plant level by calculating weighted averages according to the proportion of leaf types in the canopy. We performed this upscaling to account for spatial variation in both physiology and spectral reflectance across leaves and ensure that intra-crown variation was considered.

Physiological and spectral progression of oak wilt and drought stress. In all treatments of the potted experiment, trees with larger stem basal perimeters developed visible symptoms of stress earlier ($P < 0.001$, *SI Appendix*, Appendix S3), likely due to higher transpiration rates. The effect of stem size on symptom development rates was highest in trees infected with oak wilt that remained well watered (OW treatment). As a result, we observed large variability in symptom development rates (*SI Appendix*, Appendix S3) and physiological decline within treatments. To isolate the influence of treatments rather than inter-individual variation in size, we represented time as a function of number of days since the start of visible symptoms (Fig. 2*B*). This approach also allowed us to assess physiological state before, and after visible symptoms appeared. To assess physiological differences among oak wilt, drought, and their combined stress, we built generalized (GLM) and linear (LM) models (64) with each physiological process (VWC, RWC, LRC, EL, water potential, and Fv/Fm) as response variables and the interaction between treatment and days since the start of visible symptom appearance as predictors. We used GLMs when response variables could not be transformed to meet LM assumptions. We also built an additional model with the proportion of healthy leaves as the response variable to assess whether treatments differed in the timing and rates of symptom development.

To assess whether spectra changed in response to stress, we explored the differences in leaf or canopy spectra in the potted experiment between control and treated trees for each day that we also measured canopy reflectance with the multispectral UAV (days 13, 33, 48, 62). As comparisons of reflectance at each measured wavelength would inflate chances of false positives, we only compared a subset of wavelengths. Wavelengths were selected with a self-designed mathematical function (*SI Appendix*, Appendix S4) that used the difference in reflectance from one wavelength to the next to determine the number of wavelengths (i.e., nanometers) to skip. Thus, if two nearby wavelengths had similar reflectance, the second wavelength would be skipped to find a farther wavelength with less similar reflectance. The function also considered a minimum (5 nm) and maximum (40 nm) distance between candidate wavelengths to constrain the magnitude of the selective jumps. This procedure reduced the number of selected wavelengths from 2000 to 94 wavelengths while still representing the shape of a plant reflectance spectrum across the 400 to 2,400 nm range. To further reduce chances of false positives, we only considered differences between treatments to be significant at *P*-values lower than 0.01.

Spectral prediction of physiology. We built partial least square regression (PLSR) models (65) to test whether processes of plant dysfunction such as dehydration, cellular death, and cell content leakage could be detected from spectral reflectance data. Using the dataset from the outdoor potted experiment, we built models following a 100-iteration, 10-fold validation approach; each physiological variable (VWC, RWC, LRC, EL, water potential, Fv/Fm) was a response variable and all wavelengths resampled at 1 nm were predictors. For each physiological model, each iteration randomly divided the data into 10 groups and used 9 groups to train a PLSR model. The iteration of that model was then tested against the remaining group and its performance was assessed based on Rms error of prediction in percentage (RMSEP), R^2, slope, and bias. We optimized the number of components of the models based on RMSE. We assessed the overall capacity to predict a given physiological variable by calculating the median RMSEP and R^2 of the 100 iterations ran for each physiological model. Additionally, we extracted wavelength importance values based on Variable Importance in Projection (VIP, ref. 66) for each iteration for a given physiological model and calculated the overall importance of each wavelength as the median importance across all the iterations. Finally, we validated each physiological model against the independent Cedar Creek experiment dataset. This experiment's different location provides a useful setup to test whether spectral models are robust to differences among sites, experimental conditions, and causes of physiological stress. Each iteration within each physiological model was validated against the full Cedar Creek dataset. Then, we assessed the overall predictive accuracy of the models on the independent dataset by calculating the median RMSEP, R^2, slope, and bias of all 100 iterations, as above. We considered physiological models with an RMSEP of 20% or less to be acceptable for predicting physiological processes.

Previsual detection of oak wilt and drought stress. Using the dataset from the outdoor potted experiment, we determined whether spectrally predicted physiological processes could detect stress before visible symptom expression using Bayesian segmented regressions from the package *mcp* (67). These regressions identify inflection points (i.e., changes in status) and provide their location along the x-axis (days since visible symptom appearance) with CI around them. The response variables were the spectrally predicted physiological variables from PLSR models that showed RMSEP ≤20%, including VWC, RWC, LRC, EL, Fv/Fm, and WP. Because we measured leaf spectral reflectance in all trees at each sampling event, we could use our spectrally predicted physiological models to expand our physiological observations from a few trees per day to all trees across the experiment at each time point. By doing so, we fully captured the existing variability and minimized uncertainty around the inflection point. Time was expressed in days since the start of visible symptom appearance; this allowed us to determine if changes in physiology were occurring before visible symptoms appeared (day 0). We used the default prior settings where priors are informed based on data properties (minimum, mean, and maximum values of x and y variables and existing variation), which ensured good parameter estimates. We iterated each model to achieve convergence between three chains by adjusting the "adapt" parameter until the Gelman–Rubin convergence metric (Rhat) was close to 1 (67). We extracted inflection points and their CI for each treatment and variable to assess which inflection points (i.e., day of onset of physiological decline) were significantly lower than 0 (day of visible symptom appearance).

Physiological and spectral differentiation of oak wilt and drought stress. To test whether physiological stress mechanisms differed between oak wilt and drought, we assessed differences in functional xylem patterns among treatments before and after flushing emboli at the end of the experiment. Additionally, we divided OW trees between visually symptomatic and asymptomatic to distinguish patterns of early and late oak wilt disease progression. For each of the three measures, we tested differences in percent of functional xylem before flushing, percent of occluded xylem after flushing, and number of contiguous occluded xylem sections after flushing among groups using Wilcoxon rank sum tests to account for non-normal variance between groups. To test the extent to which OW trees displayed higher within-canopy physiological variability than D trees as they developed symptoms, we built linear models using within-canopy SD in RDVI as the response variable and the interaction between treatment and days since the start of symptom appearance as predictors. DxOW trees were not included in these models because our hypothesis was specifically targeted to differentiate drought from oak wilt symptoms.

Data, Materials, and Software Availability. Physiological, anatomical, and spectral records data have been deposited in DRUM (68).

ACKNOWLEDGMENTS. This project was funded by the Minnesota Invasive Terrestrial Plants and Pests Center (Legislative-Citizen Commission on Minnesota Resources, Project 00050727), the NSF ASCEND Biology Integration Institute (DBI: 2021898), the NASA Biodiversity program (Award number: 80NSSC21K1349), and the Cedar Creek Long Term Ecological Research program (DEB:1831944). The University of Minnesota, including Cedar Creek ESR, lies on the ancestral, traditional, and contemporary Land of the Dakota people. We would like to thank C. Lapadat for helping to plant trees. Thanks go to C. Godoy, D. Sannerud, and A. Villaseñor for

assistance in Cedar Creek campaigns. G.S. thanks W.M. Hammond for contributing funding to present this research at the 2022 Gordon Research Conference in Plant Vascular Biology. We also thank S. Kothari and A. Castillo-Castillo and anonymous reviewers for their comments in previous versions of this manuscript.

Author affiliations: [a]Department of Ecology, Evolution, and Behavior, University of Minnesota, St. Paul, MN 55108; [b]Agronomy Department, University of Florida, Gainesville, FL 32611; [c]Department of Plant and Microbial Biology, University of Minnesota, St. Paul, MN 55108; [d]Northern Research Station, United States Department of Agriculture Forest Service, St. Paul, MN 55108; and [e]Department of Forest Resources, University of Minnesota, St. Paul, MN 55108

1. IPBES, Summary for policymakers of the global assessment report on biodiversity and ecosystem services. *Zenodo* (2019). https://doi.org/10.5281/ZENODO.3553579 (17 June 2023)
2. IPCC, "Summary for Policymakers" in *Climate Change 2023: Synthesis Report. A Report of the Intergovernmental Panel on Climate Change. Contribution of Working Groups I, II and III to the Sixth Assessment Report of the Intergovernmental Panel on Climate Change*, Core Writing Team, H. Lee, J. Romero, Eds. (IPCC, Geneva, Switzerland, 2023), pp. 1–34.
3. W. M. Hammond *et al.*, Global field observations of tree die-off reveal hotter-drought fingerprint for Earth's forests. *Nat. Commun.* **13**, 1761 (2022).
4. N. G. McDowell *et al.*, Mechanisms of woody-plant mortality under rising drought, CO2 and vapour pressure deficit. *Nat. Rev. Earth Environ.* **3**, 41–44 (2022).
5. A. Findlater, I. I. Bogoch, Human mobility and the global spread of infectious diseases: A focus on air travel. *Trends Parasitol.* **34**, 772–783 (2018).
6. A. Gonzalez *et al.*, A global biodiversity observing system to unite monitoring and guide action. *Nat. Ecol. Evol.* **7**, 1947–1952 (2023). 10.1038/s41559-023-02171-0.
7. J. Cavender-Bares *et al.*, The hidden value of trees: Quantifying the ecosystem services of tree lineages and their major threats across the contiguous US. *PLoS Sustain. Transform.* **1**, e0000010 (2022).
8. S. Frankel, J. Juzwik, D. M. Rizzo, "North American oaks" in *Global Plant Health Assessment*, (International Society of Plant Pathology, ed. 1, 2022), pp. 152–158.
9. J. Juzwik, D. N. Appel, W. L. MacDonald, S. Burks, Challenges and successes in managing oak wilt in the United States. *Plant Dis.* **95**, 888–900 (2011).
10. J. Juzwik, D. N. Appel, "Diseases of trees in the Great Plains: Oak Wilt" in *Diseases of Trees in the Great Plains* (USDA Forest Service, Rocky Mountain Forest and Range Station, 2016), pp. 129–133.
11. B. E. Struckmeyer, C. H. Beckman, J. E. Kuntz, A. J. Riker, Plugging of vessels by tyloses and gums in wilting oaks. *Phytopathology* **44**, 148–153 (1954).
12. K. A. Yadeta, B. P. Thomma, The xylem as battleground for plant hosts and vascular wilt pathogens. *Front. Plant Sci.* **4**, 1–12 (2013).
13. B. Fallon *et al.*, Spectral differentiation of oak wilt from foliar fungal disease and drought is correlated with physiological changes. *Tree Physiol.* **40**, 377–390 (2020).
14. G. Sapes *et al.*, Canopy spectral reflectance detects oak wilt at the landscape scale using phylogenetic discrimination. *Remote Sensing Environ.* **273**, 112961 (2022).
15. J. Pontius, M. Martin, L. Plourde, R. Hallett, Ash decline assessment in emerald ash borer-infested regions: A test of tree-level, hyperspectral technologies. *Remote Sensing Environ.* **112**, 2665–2676 (2008).
16. A. Lausch *et al.*, Forecasting potential bark beetle outbreaks based on spruce forest vitality using hyperspectral remote-sensing techniques at different scales. *Forest Ecol. Managem.* **308**, 76–89 (2013).
17. R. Ogaya, A. Barbeta, C. Başnou, J. Peñuelas, Satellite data as indicators of tree biomass growth and forest dieback in a Mediterranean holm oak forest. *Ann. Forest Sci.* **72**, 135–144 (2015).
18. P. Asner *et al.*, A spectral mapping signature for the rapid ohia death (ROD) pathogen in Hawaiian Forests. *Remote Sensing* **10**, 1–14 (2018).
19. P. J. Zarco-Tejada *et al.*, Previsual symptoms of Xylella fastidiosa infection revealed in spectral plant-trait alterations. *Nat. Plants* **4**, 432–439 (2018).
20. M.-D. Iordache, V. Mantas, E. Baltazar, K. Pauly, N. Lewyckyj, A machine learning approach to detecting pine wilt disease using airborne spectral imagery. *Remote Sensing* **12**, 2280 (2020).
21. A. Hornero *et al.*, Modelling hyperspectral- and thermal-based plant traits for the early detection of Phytophthora-induced symptoms in oak decline. *Remote Sensing Environ.* **263**, 112570 (2021).
22. L. Cotrozzi, Spectroscopic detection of forest diseases: A review (1970–2020). *J. For. Res.* **33**, 21–38 (2022).
23. J. A. Guzmán Q. *et al.*, Mapping oak wilt disease from space using land surface phenology. *Remote Sens. Environ.* **298**, 113794 (2023).
24. C. Bhuiyan, R. P. Singh, F. N. Kogan, Monitoring drought dynamics in the Aravalli region (India) using different indices based on ground and remote sensing data. *Int. J. Appl. Earth Obs. Geoinf.* **8**, 289–302 (2006).
25. L. Cotrozzi *et al.*, Using foliar spectral properties to assess the effects of drought on plant water potential. *Tree Physiol.* **37**, 1582–1591 (2017).
26. P. D. Dao, Y. He, C. Proctor, Plant drought impact detection using ultra-high spatial resolution hyperspectral images and machine learning. *Int. J. Appl. Earth Obs. Geoinf.* **102**, 102364 (2021).
27. W. Jiao, L. Wang, M. F. McCabe, Multi-sensor remote sensing for drought characterization: Current status, opportunities and a roadmap for the future. *Remote Sensing Environ.* **256**, 112313 (2021).
28. D. Marusig *et al.*, Correlation of field-measured and remotely sensed plant water status as a tool to monitor the risk of drought-induced forest decline. *Forests* **11**, 77 (2020).
29. J. Penuelas, I. Filella, C. Biel, L. Serrano, R. Save, The reflectance at the 950–970 nm region as an indicator of plant water status. *Int. J. Remote Sensing* **14**, 1887–1905 (1993), 10.1080/01431169308954010.
30. P. J. Zarco-Tejada *et al.*, Divergent abiotic spectral pathways unravel pathogen stress signals across species. *Nat. Commun.* **12**, 6088 (2021).
31. E. Weingarten *et al.*, Early detection of a tree pathogen using airborne remote sensing. *Ecol. Appl.* **32**, e2519 (2022).
32. C. R. Guadagno *et al.*, Dead or alive? Using membrane failure and chlorophyll fluorescence to predict mortality from drought. *Plant Physiol.* **175**, 223–234 (2017).
33. J. Martinez-Vilalta, W. R. L. Anderegg, G. Sapes, A. Sala, Greater focus on water pools may improve our ability to understand and anticipate drought-induced mortality in plants. *New Phytol.* **223**, 22–32 (2019).
34. G. Sapes *et al.*, Plant water content integrates hydraulics and carbon depletion to predict drought-induced seedling mortality. *Tree Physiol.* **39**, 1300–1312 (2019).
35. M. Mantova, P. E. Menezes-Silva, E. Badel, H. Cochard, J. M. Torres-Ruiz, The interplay of hydraulic failure and cell vitality explains tree capacity to recover from drought. *Physiol. Plant.* **172**, 247–257 (2021).
36. S. P. Serbin *et al.*, Remotely estimating photosynthetic capacity, and its response to temperature, in vegetation canopies using imaging spectroscopy. *Remote Sensing Environ.* **167**, 78–87 (2015).
37. A. Onofri, P. Benincasa, M. B. Mesgaran, C. Ritz, Hydrothermal-time-to-event models for seed germination. *Eur. J. Agronomy* **101**, 129–139 (2018).
38. H. Lambers, F. S. Chapin III, T. L. Pons, *Plant Physiological Ecology* (Springer, ed. 2, 2009).
39. O. L. Lange, R. Lösch, E.-D. Schulze, L. Kappen, Responses of stomata to changes in humidity. *Planta* **100**, 76–86 (1971).
40. H. A. Snyman, W. L. J. Van Rensburg, W. D. Venter, Transpiration and water-use efficiency in response to water stress in Themeda triandra and Eragrostis lehmanniana. *South African J. Botany* **63**, 55–59 (1997).
41. W. M. Hammond *et al.*, Dead or dying? Quantifying the point of no return from hydraulic failure in drought-induced tree mortality. *New Phytol.* **223**, 1834–1843 (2019).
42. M. Mantova, S. Herbette, H. Cochard, J. M. Torres-Ruiz, Hydraulic failure and tree mortality: from correlation to causation. *Trends Plant Sci.* **27**, 335–345 (2022).
43. G. Sapes, A. Sala, Relative water content consistently predicts drought mortality risk in seedling populations with different morphology, physiology and times to death. *Plant Cell Environ.* **44**, 3322–3335 (2021).
44. G. L. Beier, B. W. Held, C. P. Giblin, J. Cavender-Bares, R. A. Blanchette, American elm cultivars: Variation in compartmentalization of infection by Ophiostoma novo-ulmi and its effects on hydraulic conductivity. *Forest Pathol.* **47**, e12369 (2017).
45. J. Oliva, J. Stenlid, J. Martinez-Vilalta, The effect of fungal pathogens on the water and carbon economy of trees: Implications for drought-induced mortality. *New Phytol.* **203**, 1028–1035 (2014).
46. K. R. Hargrave, K. J. Kolb, F. W. Ewers, S. D. Davis, Conduit diameter and drought-induced embolism in Salvia-Mellifera Greene (Labiatae). *New Phytol.* **126**, 695–705 (1994).
47. P. Fu, K. Meacham-Hensold, K. Guan, J. Wu, C. Bernacchi, Estimating photosynthetic traits from reflectance spectra: A synthesis of spectral indices, numerical inversion, and partial least square regression. *Plant Cell Environ.* **43**, 1241–1258 (2020).
48. P. Trifilò, E. Abate, F. Petruzzellis, M. Azzarà, A. Nardini, Critical water contents at leaf, stem and root level leading to irreversible drought-induced damage in two woody and one herbaceous species. *Plant Cell Environ.* **46**, 119–132 (2023).
49. S. Trueba *et al.*, Thresholds for leaf damage due to dehydration: Declines of hydraulic function, stomatal conductance and cellular integrity precede those for photochemistry. *New Phytol.* **223**, 134–149 (2019).
50. J. Juzwik, J. O'Brien, C. Evenson, P. Castillo, G. Mahal, Controlling spread of the oak wilt pathogen (Ceratocystis fagacearum) in a Minnesota Urban Forest Park Reserve. *AUF* **36**, 171–178 (2010).
51. J.-L. Roujean, F.-M. Breon, Estimating PAR absorbed by vegetation from bidirectional reflectance measurements. *Remote Sensing Environ.* **51**, 375–384 (1995).
52. J. Juzwik, An oak wilt primer. *Int. Oaks* **11**, 14–20 (2000).
53. A. Galieni *et al.*, Past and future of plant stress detection: An overview from remote sensing to positron emission tomography. *Front. Plant Sci.* **11**, 609155 (2021).
54. J. Cavender-Bares *et al.*, Integrating remote sensing with ecology and evolution to advance biodiversity conservation. *Nat. Ecol. Evol.* **6**, 506–519 (2022).
55. H. Hartmann *et al.*, Research frontiers for improving our understanding of drought-induced tree and forest mortality. *New Phytol.* **218**, 15–28 (2018).
56. N. Garcia-Forner, A. Sala, C. Biel, R. Savé, J. Martínez-Vilalta, Individual traits as determinants of time to death under extreme drought in Pinus sylvestris L. *Tree Physiol.* **36**, 1196–1209 (2016).
57. J. Cavender-Bares, F. A. Bazzaz, Changes in drought response strategies with ontogeny in Quercus rubra: Implications for scaling from seedlings to mature trees. *Oecologia* **124**, 8–18 (2000).
58. R Core Team, R: A Language and Environment for Statistical Computing (R version 3.5, R Foundation for Statistical Computing, Vienna, Austria, 2020). https://www.R-project.org/. Accessed 1 October 2021.
59. J. E. Meireles, A. K. Schweiger, J. Cavender-Bares, spectrolab: Class and Methods for Hyperspectral Data. (R package version 0.0.2, The Comprehensive R Archive Network, 2017). https://CRAN.R-project.org/package=spectrolab. Accessed 1 October 2021.
60. QGIS Development Team, QGIS Geographic Information System (Version 3.22 LTR Codename "Białowieża", QGIS Association, 2009). https://www.qgis.org. Accessed 1 October 2021.
61. M. Kaufmann, Evaluation of the pressure chamber technique for estimating plant water potential of forest tree species. *Forest Sci.* **14**, 369–374 (1968).
62. A. L. Jacobsen, R. B. Pratt, F. W. Ewers, S. D. Davis, Cavitation resistance among 26 chaparral species of Southern California. *Ecol. Monographs* **77**, 99–115 (2007).
63. C. A. Schneider, W. S. Rasband, K. W. Eliceiri, NIH Image to ImageJ: 25 years of image analysis. *Nat. Methods* **9**, 671–675 (2012).
64. K. V. Mardia, J. T. Kent, J. M. Bibby, *Multivariate Analysis* (Academic Press, 1979).
65. S. Wold, M. Sjöström, L. Eriksson, PLS-regression: A basic tool of chemometrics. *Chemometr. Intell. Lab. Syst.* **58**, 109–130 (2001).
66. M. Kuhn, Building predictive models in R using the caret Package. *J. Statist. Softw.* **28**, 1–26 (2008).
67. J. K. Lindeløv, mcp: An R package for regression with multiple change points. Open Science Framework (2020), https://doi.org/10.31219/osf.io/fzqxv (26 March 2023).
68. G. Sapes *et al.*, Data and Code for Mechanistic links between physiology and spectral reflectance enable pre-visual detection of oak wilt and drought stress. Data Repository for the University of Minnesota. https://doi.org/10.13020/0bt3-pd25. Deposited 21 December 2023.